Supporting Information

Gepshtein et al. 10.1073/pnas.1204109110

SI Methods

Templates of Sensitivity Change. The similarity of measured and predicted changes of sensitivity was measured using the templates illustrated in Fig. 6.

For the stimulus account, templates were determined by stimulus statistics (Fig. 2*A*). The boundaries of template regions were 11 and 45 deg/s for the region of expected gain, 1.4 and 0.36 deg/s for the region of expected loss. No changes were expected between the speeds of 0.36 and 11 deg/s.

For the system account, the template consisted of four regions where the system account predicted gains and losses of sensitivity (Fig. S3*B*). Because the predictions depended on locations of maximal-sensitivity sets $\mathcal{M}$, the boundaries between regions were derived in two steps. First, parameters of $\mathcal{M}$ were estimated for each stimulus context, as explained in section *Modeling Spatiotemporal Sensitivity* (*Methods*). Second, five boundaries were placed as explained in Fig. S3*B*.

Spatial boundary S was placed between the spatial asymptotes of $\mathcal{M}_h$ and $\mathcal{M}_l$ (i.e., the asymptotes of $\mathcal{M}$ parallel to the spatial-frequency axis of the stimulus space). Temporal boundaries T_1 and T_2 were parallel to the temporal-frequency axis: T_1 was placed between the temporal asymptotes of $\mathcal{M}_h$ and $\mathcal{M}_l$, and T_2 limited the region of large expected changes of sensitivity at high temporal frequencies. Speed boundaries V_1 and V_2 were drawn diagonally, through the point of intersection of $\mathcal{M}_h$ and $\mathcal{M}_l$ represented in Fig. S3 by the yellow disk.

Because parameters of $\mathcal{M}$ differed across observers, the same structure of template generated different shapes of template regions in different observers (Fig. 5). Even though system templates were derived from measured observer characteristics, the measured changes of sensitivity captured by the four regions of the system template could be radically different from the changes predicted by the system account. For example, if the measured distribution of sensitivity had shifted in the direction opposite to that predicted by the system account, the positive and negative measured changes of sensitivity would be found in the regions where negative and positive changes were expected, respectively, yielding negative evidence $E_\forall$ for the system account (Eq. **2**).

Analysis of Sensitivity Changes Within Templates. Results would agree with predictions if the measured gains were consistently found where gains were expected, and the measured losses were consistently found where losses were expected. The agreement was quantified using cumulative index

$$\Delta_\forall = \Delta_G - \Delta_L, \qquad \textbf{[S1]}$$

where Δ_G and Δ_L were the mean changes of sensitivity on the nodes of stimulus grid for which gains and losses of sensitivity were expected, respectively. Because Δ_G is expected to be positive, and Δ_L is expected to be negative, the larger the value of $\Delta_\forall$ the better the match to template. Individual values of $\Delta_\forall$ for the system account are displayed in the bottom right corner of every panel in Fig. 5. Errors of $\Delta_\forall$ were estimated for every observer. Measured sensitivity changes were resampled within template regions, and distributional properties of $\Delta_\forall$ were computed from the resampled regional sensitivity changes. The resampling analysis showed that the measured magnitudes of $\Delta_\forall$ were unlikely to arise by chance ($P < 0.01$).

Cumulative evidence for alternative accounts of adaptation was computed on the nodes of the stimulus grid according to Eq. **2**. For the system account, the two components of cumulative evidence were

$$E_{(+)} = G_1 - L_2 \qquad \textbf{[S2]}$$

$$E_{(-)} = L_1 - G_2, \qquad \textbf{[S3]}$$

where G_i and L_i stand for the mean gains and mean losses of sensitivity in template regions 1 and 2, indicated by the subscripts (Fig. 6*A*). For the stimulus account, component $E_{(+)}$ was the same as in Eq. **S2**. However, component $E_{(-)}$ differed from Eq. **S3** because now cumulative evidence had to incorporate the predicted absence of sensitivity change in the neutral region (white region labeled $\ominus$ in Fig. 6*B*):

$$E_{(-)} = L_1 - G_2 - N, \qquad \textbf{[S4]}$$

where N was the mean absolute change of sensitivity in the neutral region.

Confidence intervals for cumulative evidence $E_\forall$ were estimated for every observer separately for the system account and the stimulus account (Fig. 6). Individual sensitivity changes were resampled separately on the nodes that supported either account (E_+) and the nodes that opposed either account (E_-), and then cumulative evidence $E_\forall = E_{(+)} - E_{(-)}$ was computed from the resampled sensitivity changes. Significance of $E_\forall$ was evaluated using 95% and 99% confidence intervals.

Outline of the System Account of Visual Adaptation

Here we summarize key steps in derivation of the optimal set: a theoretical equivalent of the measured maximal-sensitivity curve labeled "max" in Fig. 1*D*. A complete derivation is presented in Gepshtein et al. (1). The theory predicts that the shape of the curve remains invariant under changes in statistics of stimulation, but the position of the curve in the stimulus space depends on stimulus statistics (Fig. 2*C*).

Joint Measurement Uncertainty. Neurons tuned to stimuli in different parts of the domain of spatiotemporal contrast sensitivity function (the "stimulus space") have receptive fields of different size. The neurons are therefore expected to convey information about stimulus parameters with different uncertainty (different precision). According to the uncertainty principle formulated by Gabor (2), uncertainty of measuring stimulus frequency content is low for large receptive fields and high for small receptive fields. Conversely, the uncertainty of measuring stimulus location is high for large receptive fields and low for small receptive fields. The argument applies equally to the spatial and temporal aspects of stimuli. Assuming that the same neurons are used to measure the locations and frequency content of stimuli, Gepshtein et al. (1) derived a joint uncertainty function equation 7 in ref. 1) that characterizes the distribution of expected uncertainty of measurement across the stimulus space.

Invariant Shape of the Optimal Set. Minima of the joint uncertainty function for every speed form the "optimal set" of spatiotemporal measurement—a set of stimulus conditions at which individual speeds are measured with minimal uncertainty. This optimal set may have a variety of shapes in the stimulus space, depending on how the components of measurement uncertainty combine in the joint uncertainty function. However, the optimal set is an abstraction that disregards two basic facts of biological vision.

First, the extent of neuronal receptive fields across speeds is not negligible. Visual information is necessarily integrated across speeds. When this constraint is taken into account, the shape of the optimal set has an invariant shape: a rectangular hyperbola in the parameter space (equation 10 in ref. 1).

Position of the Optimal Set. Second, different speeds are not equally important for perception. Because of its limited resources, biological vision cannot optimize measurement of every speed. Visual systems must determine how to allocate resources across stimuli, according to stimulus importance or frequency of the stimulus in the environment. In the framework of Gepshtein et al. (1), the most suitable conditions for speed estimation with limited resources are obtained when contributions of individual speeds are weighted according to the distribution of speed in the stimulation. In effect, the position of the optimal set in the stimulus space changes together with the distribution of speed in the environment (equation 21 and figure 8 in ref. 1). For example, an increase in the mean stimulus speed leads to a shift of the optimal set, as illustrated in Fig. 2*C*. [The space-time representation of stimuli used by Gepshtein et al. (1) is converted to the spectral representation using standard assumptions (3, 4) summarized in ref. 1, pp 14–15.]

Changes in other aspects of stimulus statistics also affect the position of the theoretical optimal set. In this study we focus on changes in the mean speed of stimulation, because the ensuing pattern of sensitivity changes is highly distinctive: the gains and losses of sensitivity expected by the system account within speeds (Fig. 2*C*) stand in stark contrast to the monotonic transition from losses to gains across speeds expected by the stimulus account (Fig. 2*B*).

The theoretical optimal set corresponds to the empirical maximal-sensitivity set (represented by curve "max" in Fig. 1*D* and by the white crosses in Fig. 3*B*). Notice that, according to the system account, the prediction is that changes in stimulus statistics lead to a shift of the optimal set, and not to a rigid translation of the distribution of sensitivity in the stimulus space. As the position of the optimal set changes, the sensitivity is organized around the new location of the optimal set in a way that is generally different from a rigid translation of the distribution of sensitivity.

1. Gepshtein S, Tyukin I, Kubovy M (2007) The economics of motion perception and invariants of visual sensitivity. *J Vis* 7(8):8.1–18.
2. Gabor D (1946) Theory of communication. *Institution of Electrical Engineers* 93(Part III): 429–457.
3. Nakayama K (1985) Biological image motion processing: A review. *Vision Res* 25(5): 625–660.
4. Heess N, Bair W (2010) Direction opponency, not quadrature, is key to the 1/4 cycle preference for apparent motion in the motion energy model. *J Neurosci* 30(34): 11300–11304.

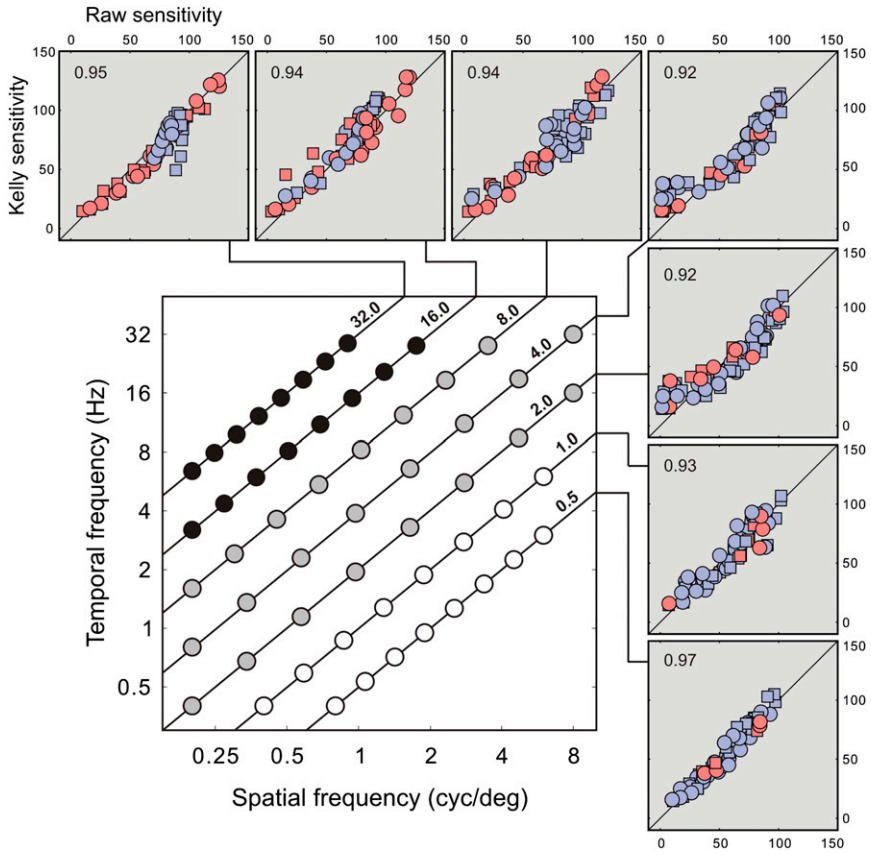

Fig. S1. Results of experiment 2: Sensitivity estimates within speeds. The central panel reproduces the stimulus grid from Fig. 3*A*. Disk locations represent the tested spatiotemporal stimulus conditions, and disk colors represent whether stimulus frequency increased (black), decreased (white), or did not change (gray) in the high-speed context relative to the low-speed context. (*Insets*) These seven panels contain scatter plots of sensitivity at the seven stimulus speeds using the fitted Kelly functions vs. the "raw" estimates produced by our measurement procedure. Symbol shapes indicate the context of stimulation: circles for high speed and squares for low speed. Displays of correlation coefficients on top left of every inset indicate that the raw estimates of sensitivity were well approximated by Kelly functions. The data deviating from the diagonal line indicate conditions where the Kelly model fitted sensitivity estimates less successfully. (We found that most of these conditions were localized at the top right of the main panel, i.e., at high spatiotemporal frequencies. These conditions had only a small effect on the template-matching computation for Fig. 6*A* because they were outside of the regions where gains and losses of sensitivity were expected by the system account.) Adaptation caused both increments and decrements of sensitivity within every tested stimulus speed, represented by color: red for increments and blue for decrements of sensitivity change, in the high-speed context relative to the low-speed context.

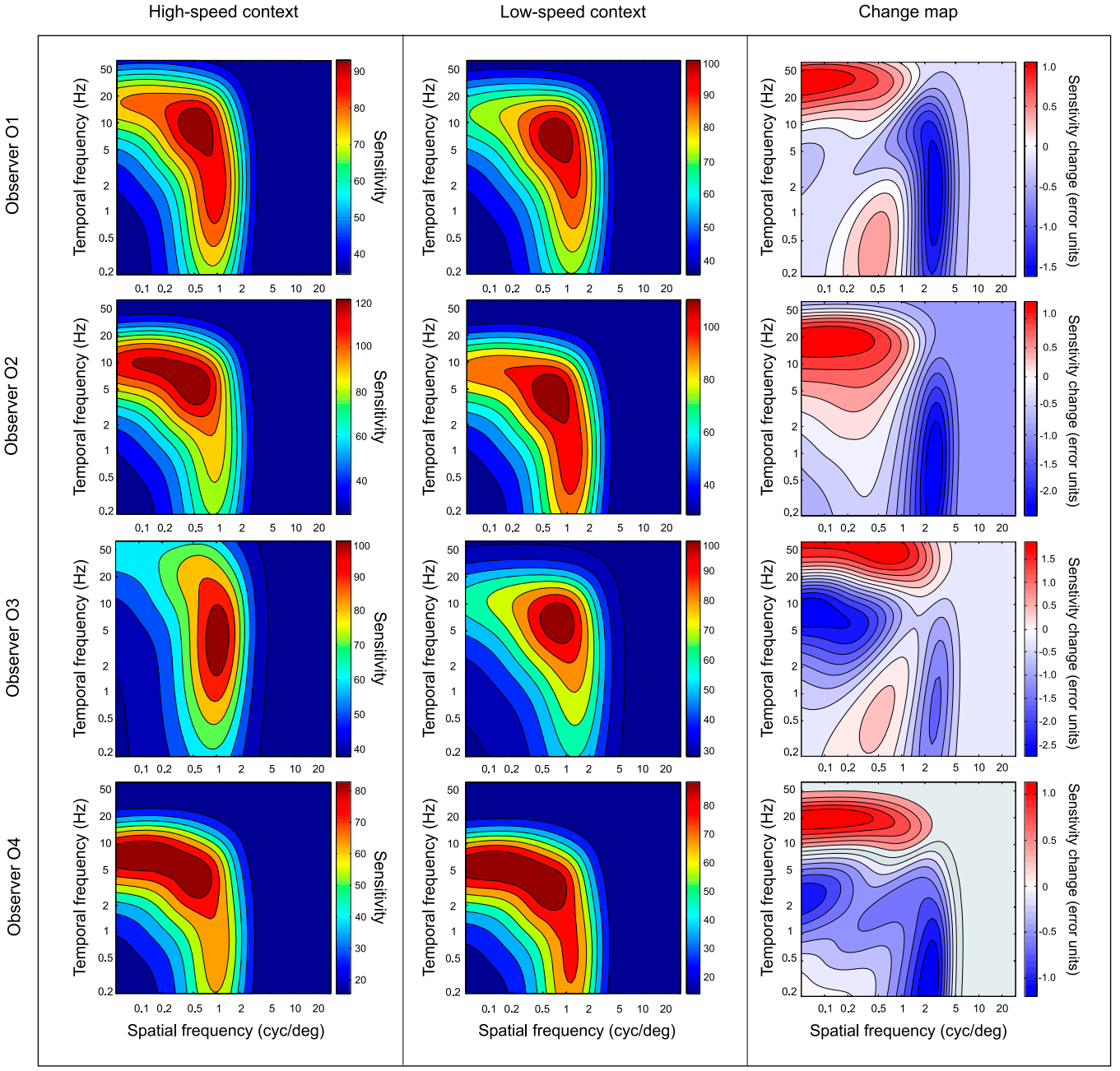

Fig. S2. Sensitivity maps for all observers are displayed for the high-speed and low-speed contexts in the first and second columns, respectively, using the same convention as in Fig. 4*A*. Change maps for all observers are displayed in the third column. In contrast to Fig. 5, here the magnitudes of sensitivity change are scaled by posterior error estimates provided by the Bayesian estimation procedure (*Methods*).

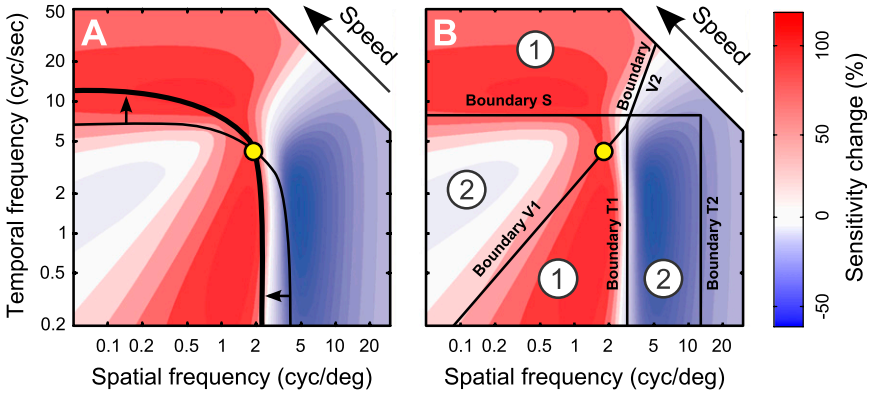

Fig. S3. Derivation of the system template of sensitivity change. (*A*) The black curves represent conditions of maximal sensitivity predicted by the system account of adaptation (1) for the low-speed (thin curve) and high-speed (thick curve) environments. The yellow disk marks the intersection of the curves. Focal changes of sensitivity are expected in specific regions of the change map relative to the maximal sensitivity curves. (The theoretical change map in the background marks the expected gains and losses of sensitivity using shades of red and blue, respectively, i.e., using the same conventions as Figs. 4*B* and 5.) As stimulus context changes from low-speed to high-speed, the horizontal branch of the curve moves up on the temporal axis (upward black arrow), creating regions of gains and losses of sensitivity at high and low temporal frequencies, respectively. Similarly, the vertical branch of the curve moves down on the spatial axis (leftward black arrow), creating regions of gains and losses of sensitivity at low and high spatial frequencies, respectively. (*B*) The black lines indicate boundaries between the regions where distinct changes of sensitivity are expected. Spatial boundary S separates gains from losses at low spatial frequencies, and temporal boundary T1 separates gains from losses at low temporal frequencies. Speed boundaries V1 and V2 separate regions across speeds, and temporal boundary T2 limits the region of expected sensitivity loss at high spatial frequencies.